Topological thermoelectrics

Chenguang Fu ⓘD , Yan Sun, and Claudia Felser

COLLECTIONS

View Online   Export Citation   CrossMark

ARTICLES YOU MAY BE INTERESTED IN

Topological thermoelectrics

View Online Export Citation CrossMark

Chenguang Fu,[a] (iD) Yan Sun, and Claudia Felser[b]

AFFILIATIONS

Max Planck Institute for Chemical Physics of Solids, 01187 Dresden, Germany

Note: This paper is part of the Special Issue on New Perspectives on Emerging Advanced materials for Sustainability.
[a]Author to whom correspondence should be addressed: Chenguang.Fu@cpfs.mpg.de
[b]Email: Claudia.Felser@cpfs.mpg.de

ABSTRACT

Since the first-generation three-dimensional topological insulators were discovered in classic thermoelectric systems, the exploration of novel topological materials for advanced thermoelectric energy conversion has attracted increasing attention. The rapid developments in the field of topological materials, from topological (crystalline) insulators, Dirac/Weyl semimetals, to magnetic Weyl semimetals, have offered a variety of exotic electronic structures, for example, topological surface states, linear Dirac/Weyl bands, and large Berry curvature. These topological electronic structures provide a fertile ground to advance different kinds of thermoelectric energy conversion based on the Seebeck effect, magneto-Seebeck effect, Nernst effect, and anomalous Nernst effect. In this Perspective, we present a vision for the development of different topological materials for various thermoelectric energy conversion applications based on their specific topological electronic structures. Recent theoretical calculations and experimental works have been summarized to demonstrate practical routes for this new field. Further outlook on scientific and technological challenges and opportunities with regard to topological thermoelectrics are offered.

INTRODUCTION

Solid-state thermoelectric (TE) technology enables direct energy conversion between heat and electricity, which provides a potential solution for the current energy crisis.[1,2] The conversion efficiency of a TE material is gauged by a dimensionless figure of merit: $zT = S^2 T/\rho(\kappa_e + \kappa_{ph})$, where S is the Seebeck coefficient or thermopower, T is the absolute temperature, ρ is the electrical resistivity, and κ_e and κ_{ph} are the electronic and phonon components of the total thermal conductivity κ, respectively.[3] Since Seebeck discovered the first TE effect, i.e., Seebeck effect, in 1821,[4] TE research has experienced several major advances. In the 1950s, the milestone concepts of narrow band gap semiconductors and solid solutions[5] led to the discovery of $(Bi,Sb)_2(Te,Se)_3$ and $Bi_{1-x}Sb_x$ TE systems, which have become the most successful TE materials for power generation and refrigeration near and below room temperature.[3] The latest major advance started in the 1990s, and its development continues to date based on the novel ideas of low-dimensionality,[6,7] phonon-glass electron-crystal paradigm,[8] electronic structure engineering,[9–11] hierarchical phonon scattering,[12] and point defect

engineering,[13] to name a few. Nowadays, dozens of semiconductor systems have been discovered as good TE materials with a peak zT of ~1–2.[2,14,15]

Great achievements have been made in TE research in the past 30 years; however, further improvement in the peak zT of good TE materials seems to become more difficult. Specifically, the κ_{ph} of most TE materials can be suppressed to their minimum value through either hierarchical phonon scattering[12,15] or phonon engineering[16] to effectively impede the propagation of heat-carrying phonons. Further improvement of zT relies on enhancing the electrical power factor, which is defined as S^2/ρ. Current band structure engineering strategies,[17,18] such as distortion of the electronic density of states,[10] convergence of electronic bands,[11,19] modification of band effective mass,[20,21] and tuning of carrier scattering potentials,[22] have been proven effective in improving the power factor. However, it is still very difficult to achieve several times enhancement in the optimal power factor of a TE material once the optimal carrier concentration has been reached.

In the past 15 years, there have also been surging research activities on quantum topological materials (TMs). Based on the

emerging topological band theory,[23,24] exotic electronic structures and physical properties have been identified in TMs,[25–27] including the topology-protected surface state, linear Dirac/Weyl band dispersions, Fermi arc (an unclosed line that starts from one Weyl point and ends at the other with opposite chirality[27]), chiral anomaly, ultrahigh carrier mobility, giant magnetoresistance, and large Berry curvature (characterizing the wave-function entanglement between the conduction and valence bands[27]). These exotic physical properties make TMs very appealing platforms for exploring novel materials targeting functional applications, for example, dissipative power electronics,[28] novel photocatalysts and electrocatalysts for water splitting,[29–31] advanced spintronic devices,[32] and thermoelectrics.[33] Specifically, TMs have a rather close relationship with TE materials. The first-generation three-dimensional (3D) topological insulators (TIs) were discovered in the most famous TE systems: $Bi_{1-x}Sb_x$ and $(Bi,Sb)_2(Te,Se)_3$.[34,35] Topological crystalline insulators[36] were discovered in the chalcogenides $Pb_{1-x}Sn_xTe$,[37–39] which exhibit good TE performance in the intermediate temperature.[40] Later, Dirac fermions were discovered experimentally in semimetal Cd_3As_2,[41,42] which was long known for its high carrier mobility[43] and low thermal conductivity.[44] The magneto-TE and thermomagnetic properties of Cd_3As_2 had also been studied, and a strong response was observed even at magnetic field below 1 T.[45] Pentatelluride $ZrTe_5$, also identified as a Dirac semimetal[46] with temperature-induced Lifshitz transition,[47] attracted the attention of TE researchers around the 2000s owing to its low thermal conductivity and moderate Seebeck coefficient.[48,49] The TE properties of Kagomé-lattice $Co_3Sn_2S_2$, a very recently discovered magnetic Weyl semimetal,[50–52] were also studied in the past years.[53] In all, the topological properties are likely to have a close relationship with the TE properties and they usually occur concomitantly in the same material system. Thus, bridging these two fields is very appealing, which would prompt the understanding of the topological band structure from the TE transport measurements and also advance the discovery of novel TMs for energy conversion.

There are several excellent reviews on the relation between TIs and TE materials.[33,54–57] In this Perspective, we offer a vision for the development of novel TMs, including TIs and non-magnetic and magnetic topological semimetals (TSMs), for different kinds of TE energy conversion, as outlined in Fig. 1. In the first section, we briefly introduce the successful strategies used in current TE research and discuss possible new ways to improve the TE performance. In the second section, with regard to the topological electronic structure of TMs, their potential for energy conversion based on different kinds of TE effects is summarized. In the last section, we summarize possible challenges and opportunities in the studies of topological thermoelectrics. Last but not least, the literature is vast in the topic of TMs and TEs; thus, we regret not having covered all the works and may have omitted important information.

THERMOELECTRIC EFFECTS

Seebeck effect

After 30 years of dynamic development, the optimization of TE performance for new semiconductors has been well established. First and foremost, the carrier concentration n should be optimized owing to the opposite dependencies of transport parameters on n (Fig. 2), i.e., S and ρ decrease while κ_e increases with increasing n.[1] The optimal carrier concentration n_{opt} of a TE semiconductor,
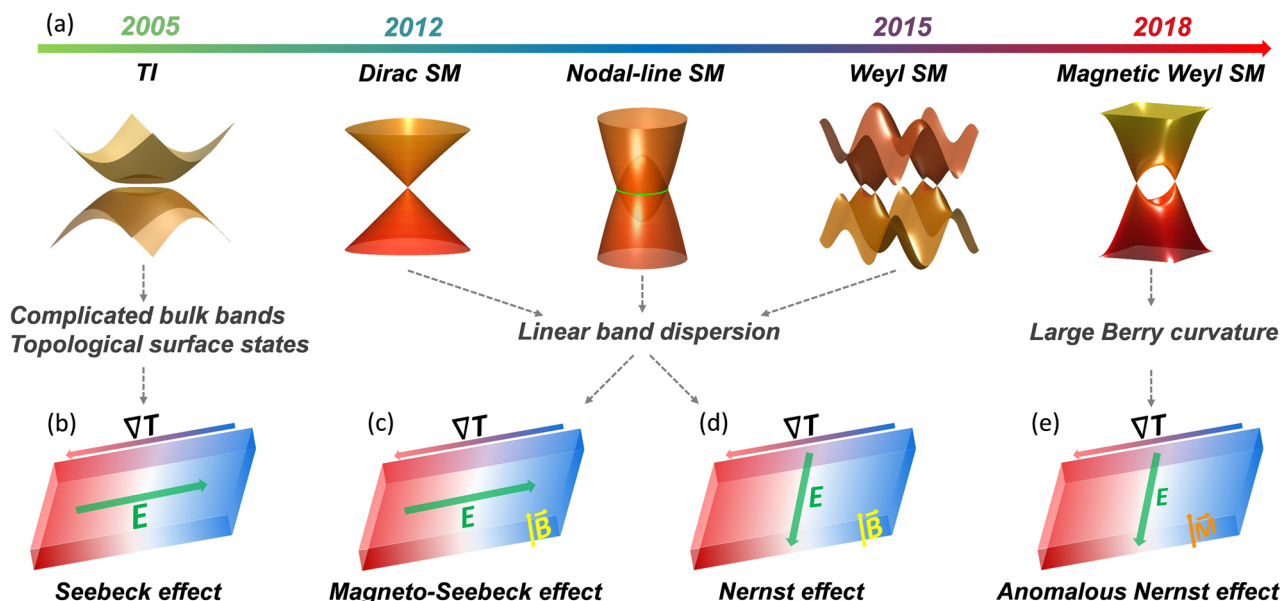
FIG. 1. (a) Development of TMs from TIs to various TSMs and their potential for different kinds of TE effects: (b) Seebeck effect, (c) magneto-Seebeck effect, (d) Nernst effect, and (e) anomalous Nernst effect. The unique electronic structure features of TMs, making the connection to the corresponding TE effects, are highlighted, i.e., TI: complicated bulk bands and topological surface states; Dirac, nodal line, and Weyl semimetals: linear band dispersion; and magnetic Weyl semimetal: large Berry curvature.
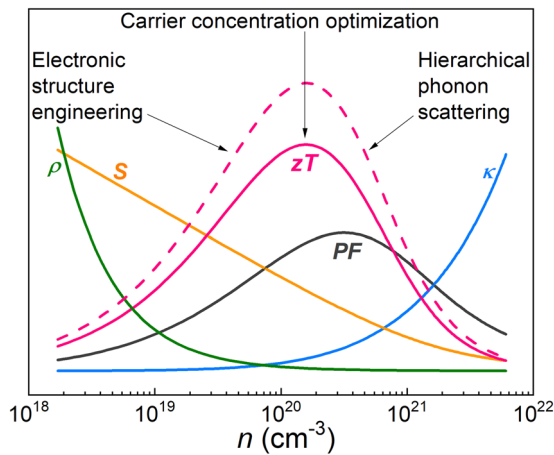
FIG. 2. Representative strategies to enhance the zT of a TE semiconductor.[1,11,12]

which is proportional to its density of states effective mass,[58] is generally in the range of 10^{19}–10^{21} cm^{-3}.[1,2] In this step, one could achieve a large enhancement of zT if the initial carrier concentration of the TE semiconductor deviates significantly from its n_{opt}. After achieving n_{opt}, further enhancement of TE performance can be realized by suppressing the phonon thermal conductivity κ_{ph} via hierarchical phonon scattering[12] or phonon engineering.[16] This is owing to the relative independence between κ_{ph} and n. In addition, one can engineer the electronic structure[10,11] of the TE semiconductor to further improve its optimal power factor. This step is more challenging and is generally directed by the calculated electronic structures and transport properties.[59] It is worth noting that n_{opt} might change in the last two steps. Therefore, further optimization of n_{opt} is sometimes necessary. When rational strategies are well designed, one could also optimize these transport parameters simultaneously to improve zT.[60,61]

Nowadays, there are many effective strategies to suppress the κ_{ph} of TE materials to approach the minimum value.[14] Here, to make an estimation of the upper limit of zT, we simply neglect the κ_{ph} term, i.e., $zT = S^2T/\rho(\kappa_e + \kappa_{ph}) < S^2T/\rho\kappa_e$. The Wiedemann–Franz (WF) law relates κ_e to ρ through the expression $\kappa_e = LT/\rho$, where L is the Lorenz number.[62] Thus, the upper limit of zT is set by S^2/L. In most good TE semiconductors, the absolute S is generally in the range of 300–100 μV/K. Specifically, Hong et $al.$ have recently reported a more narrow range of 202–230 μV/K by the big data survey of more than a hundred good TE materials.[63] The Lorenz number L is usually in the range of 1.5–2.44 × 10^{-8} W Ω K^{-2}, as set by the non-degenerate and degenerate limits.[3] These explain why the peak zT of current TE semiconductors can hardly exceed 2. Despite this, S^2/L does indicate two probable ways to improve the upper limit of zT, having either larger S or lower L or both.

The Mott formula[64] relates S to the energy-dependent electrical conductivity $\sigma(E) = n(E)$ $e\mu(E)$,[10] as follows:

$$S = \frac{\pi^2 k_B^2 T}{3e}\left(\frac{d\ln\sigma(E)}{dE}\right)_{E=E_F} = \frac{\pi^2 k_B^2 T}{3e}\left(\frac{1}{n}\frac{dn(E)}{dE} + \frac{1}{\mu}\frac{d\mu(E)}{dE}\right)_{E=E_F}.$$

(1)

According to this expression, there are two ways to improve S, i.e., increasing the energy-dependence of $n(E)$ or $\mu(E)$. Through a local distortion in the electronic density of state $g(E)$ and $n(E)$, the S of PbTe was largely enhanced with the use of the thallium impurity levels.[10] A significant increase in S was also reported in Ni-doped CoSb$_3$ owing to the strong temperature-dependence of $\mu(E)$.[65] Both successful modulations of the energy-dependence of $n(E)$ and $\mu(E)$ in PbTe and CoSb$_3$ were based on the rational selection of chemical substitution. The magnetic field provides another way to modulate the energy-dependence of $\sigma(E)$ of solid materials. In the presence of an external magnetic field, the cyclotron orbits of charge carriers can be quantized, which is directly responsible for the magnetic oscillations of the electronic properties.[66] In this scenario, the charge carriers can only occupy orbits with discrete energy values, called Landau levels.[67] The most well-known response of electronic properties to a magnetic field is magnetoresistance,[66] which can have several orders of magnitude enhancement for high-mobility semimetals, for example, Bi,[68] WTe$_2$,[69] Cd$_3$As$_2$,[70] NbP,[71] and PtSn$_4$.[72,73] The magneto-thermopower can also be significantly enhanced in Bi$_{1-x}$Sb$_x$,[74] Bi$_2$Te$_3$,[75] and Cd$_3$As$_2$.[76] Recently, the non-saturating increase in the thermopower of Dirac/Weyl semimetals in a quantizing magnetic field has been predicted.[77] Therefore, the magnetic-field-modulated energy-dependence of $\sigma(E)$ in TMs offers a probable way to enhance S.

The WF law has generally been obeyed for metals above room temperature. One important assumption of this law is that the charge carriers are scattered elastically,[62] which is generally the case for heavily doped TE semiconductors above room temperature. Therefore, in TE research, the WF law is usually employed to estimate κ_e and thus to separate κ_{ph} from κ. The violation of the WF law might occur if the carrier scattering mechanism becomes inelastic scattering. For metals or some semimetals below room temperature, the carriers are subjected to inelastic scattering, where a moderately lower Lorenz number is observed.[78] Moreover, the hydrodynamic electron flow has recently been found in 2D graphene,[79,80] in which a strong enhancement of the Lorenz number is observed. In the other 3D hydrodynamic electron flow candidates, i.e., highly conductive PdCoO$_2$[81] and Weyl semimetal WP$_2$,[78,82] a smaller Lorenz number and violation of the WF law are found. These results suggest that the emerging TM materials might provide a platform to find new TE materials with the violation of the WF law.

Nernst effect

Most of the current TE studies are focused on the Seebeck effect,[2] in which the applied temperature gradient is in parallel with the induced electric field [Fig. 1(b)]. As a result, the coupling of phonon and electron transport properties is usually unavoidable and makes the enhancement of TE performance challenging. For example, introducing multiple phonon scattering sources is an effective way to suppress κ_{ph}, which, however, could also deteriorate μ, offsetting the enhancement of zT.[14] When a magnetic field is applied perpendicular to the temperature gradient, a transverse electric field will also be generated in the orthogonal direction, which is dubbed as the Ettingshausen–Nernst effect[83] [Fig. 1(d)]. In the Nernst effect setup, the charge carriers tend to accumulate in the transverse direction, while the phonons propagate in the longitudinal direction, enabling the decoupling of the phonon and electron transport properties.

The elemental semimetal Bismuth, in which the Nernst effect was first found, still holds the record for Nernst coefficient among the studied solid materials.[84] By alloying with Sb and As, $Bi_{1-x}Sb_x$ and $Bi_{1-x}As_x$, with the lowered κ_{ph}, had been studied for Ettingshausen cooling owing to the large thermomagnetic figure of merit.[85–88] The beneficial features for Bi and its alloys to exhibit a large Nernst effect lie in the electron–hole compensation, small Fermi surface, and ultrahigh μ. These features are also found in the recently discovered non-magnetic TSMs, in which the linear band crossing near the Fermi level is the hallmark.[27,89] Therefore, non-magnetic TSMs provide a playground to find novel materials with a large Nernst effect.

The Nernst effect has shown important advantages compared to the Seebeck effect, for example, decoupling the thermal and electric transport and no need for both n-type and p-type TE materials to make the device.[90] However, the additional requirement of the magnetic field is a challenge for practical applications. Therefore, finding large Nernst response at low magnetic fields, particularly in the range where the permanent magnets can reach (below 2 T), is important.[91] Moreover, a question arises as to whether we can find materials showing the Nernst effect without the need of a magnetic field. This has also been discovered in ferromagnetic materials with a large Berry curvature.[92,93] In crystals with broken time-reversal symmetry, the Berry curvature becomes nonzero.[94] As a result, the anomalous Nernst effect (ANE) occurs when applying a temperature gradient on the ferromagnetic materials. Magnetic TSMs are a perfect host of both magnetism and topology, which thus become a promising material database for exploring the large ANE.

TOPOLOGICAL THERMOELECTRICS

TIs: Seebeck effect

TI is the first member of the big TM family.[25] The first-generation 3D TIs were discovered in the classic $Bi_{1-x}Sb_x$[34] and $(Bi,Sb)_2(Te,Se)_3$[35] TE systems. Since this discovery, the intrinsic connection between the TE performance and topological behavior has attracted considerable interest in both fields.[33,54] The main feature in the electronic structure of a TI is the topological surface state. As schematically illustrated in Figs. 3(a)–3(c), to have the topological surface state, band inversion is necessary to create anti-crossing between conduction and valence bands. With strong spin–orbit coupling (SOC), which generally occurs in heavy elements, the band gap opens and the TI occurs. In TIs, the complex non-parabolic bulk bands are highly desirable for a large Seebeck effect[95] and the heavy elements guarantee a lower κ_{ph}. These two features make TIs good candidates as high-performance TE materials based on the Seebeck effect.[33,95]

Although TIs and high-performance TEs can be found in the same material system, for example, Tetradymites,[33] they have different requirements in the location of Fermi level E_F. For high-performance TEs, E_F is generally located at the edge of either conduction or valence bands, which corresponds to the bulk transport properties. To observe the topological surface state-dominated transport properties in TIs, it is important to shift E_F to the Dirac point so that the contribution from the bulk state is suppressed.
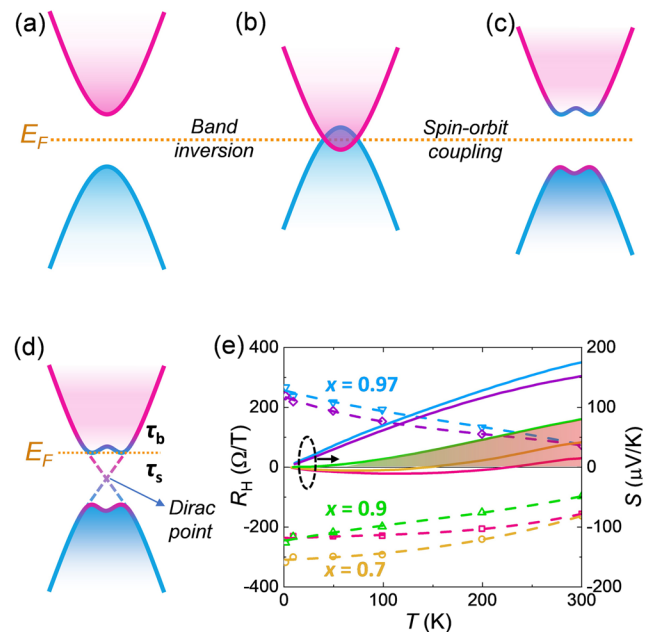

FIG. 3. (a)–(c) Schematic illustration of the evolution of the electronic structure under band inversion and spin–orbit coupling.[95] (d) Electronic structure of a representative TI with relaxation time τ_b; the dashed lines indicate the surface state with relaxation time τ_s. (e) Hall coefficient and thermopower vs temperature for the five quintuple layer $(Bi_{1-x}Sb_x)_2Te_3$ films with $0.7 \leq x \leq 0$.[96]

Nevertheless, separating the topological surface state's contribution to electrical transport is still difficult in a 3D system because the bulk state's contribution generally dominates. Only at a very low temperature, if E_F is well shifted into the forbidden gap, the transport properties might be dominated by the surface or edge states.[56]

The topological surface state-induced transport properties were studied in 2D thin films or nanostructures at low temperatures.[56] Owing to the linear dispersion for topological surface states, the relaxation time τ_s could be much larger than the corresponding bulk relaxation time τ_b, indicating that the surface states could lead to very high conductivity σ_s. Considering a scenario where E_F is located between the bulk and topological surface states, both states would contribute to the transport properties. The thermopower S can be expressed as follows:[97]

$$S = \frac{S_b G_b + S_s G_s}{G_b + G_s}, \quad (2)$$

where $G_{s,b}$ and $S_{s,b}$ are the electrical conductance and thermopower of the surface and bulk states, respectively. Assuming that E_F is located at the edge of the conduction band and above the Dirac point [Fig. 3(d)], S_b is always negative, and S_s is positive because the Dirac point appears below E_F. The relative contribution to S is then weighted by the ratio G_b/G_s. If $\tau_s \gg \tau_b$, the surface states outweigh the bulk state and contribute to a positive value of S, even though E_F is located near the conduction band. This is called the anomalous Seebeck effect, which was predicted by Xu et al. in 2014.[97]

Soon after this prediction, an experimental work on five quintuple layer $(Bi_{1-x}Sb_x)_2Te_3$ films was reported by Zhang *et al.*, where they observed a sign anomaly between Hall coefficient R_H and S.[96] As summarized in Fig. 3(e), for sample $x = 0.9$, S is typically positive, while its R_H is negative throughout the studied temperature range. This sign anomaly is attributed to the distinct transport behaviors of bulk and surface states: the surface states dominate R_H, while S is mainly determined by the bulk states.[96] Although this is still far from the predicted anomalous Seebeck effect,[96] it paves the way for experimentally exploring topological surface state-dominated TE transport behavior. More recently, a computational work on six quintuple layer Bi_2Se_3 thin films has been reported,[98] where the relaxation time of the topological surface states was predicted to be hundreds of femtoseconds, which is two orders of magnitude higher than that of the bulk states. This could provide a new experimental platform for the realization of the anomalous Seebeck effect. In all, the experimental observation of the topological surface state-dominated TE transport properties is very challenging because it requires an ideal material system with a well-modulated E_F. However, further studies in this direction are appealing. In one aspect, the synergistic measurements of longitudinal and Hall resistivities and thermopower could help to disentangle the bulk and topological surface states of TIs. In another aspect, the topological surface state-dominated TE transport properties provide a new way for TE research.

Non-magnetic TSMs: Magneto-Seebeck and Nernst effects

As 3D analogs of graphene, Dirac and Weyl semimetals are phases of matter with gapless electronic excitations that are protected by topology and symmetry.[99] As described by the massless Dirac equation, Dirac semimetals have a four-fold-degenerate Dirac point [Fig. 4(a)], which is the node crossed by linearly dispersive conduction and valence bands in 3D momentum space. By breaking either the inversion symmetry or the time-reversal symmetry, the Dirac point can be split into a pair of two-fold-degenerate Weyl points [Fig. 4(b)]. Similar to TIs, Dirac and Weyl semimetals also host topological surface states; more specifically, the Fermi arc connects the two Weyl points in the latter.[100] The bulk transport properties are more related to the linear dispersion of bands, resulting in a very small Fermi surface and effective mass and very large carrier mobility and magnetoresistance. TSMs host two types of charge carriers, i.e., electrons and holes. Under a longitudinal temperature gradient, both electrons and holes can move toward the cold side, which balances each other's contributions to the thermopower [Fig. 4(c)]. However, when a magnetic field is applied perpendicular to the temperature gradient, the Lorentz force deflects electrons and holes to opposite transverse directions, which can generate a large transverse Nernst effect [Fig. 4(d)].[84] Owing to the presence of electrons and holes, TSMs usually display very high magnetoresistance, which is even not saturating at higher magnetic fields of tens of Tesla.[69] The energy-dependence of $\sigma(E)$ can be significantly modulated under the magnetic field, providing another way to improve thermopower S.

Recently, Skinner and Fu have theoretically predicted a large and non-saturating thermopower in Dirac/Weyl semimetals subjected to a quantized magnetic field.[77] Beyond the quantum limit, the thermopower grows linearly with the field without
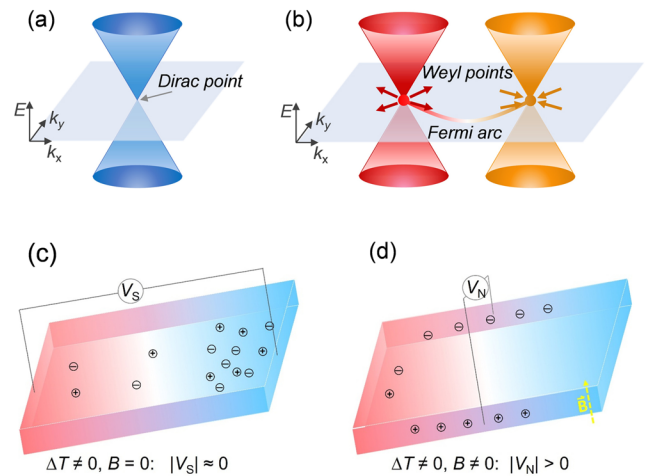

FIG. 4. (a) and (b) Sketch of the electronic structure of Dirac and Weyl semimetals, respectively. In a semimetal, the temperature gradient drives both electrons and holes to the cold side, making the overall thermopower almost zero (c); further application of a magnetic field could deflect the moving electrons and holes to opposite transverse directions, contributing to a strong transverse Nernst voltage (d).

saturation, consistent with the experimental work on Dirac semimetal $Pb_{1-x}Sn_xSe$.[101] The realization of the quantum limit in most solid materials generally requires a high magnetic field. It is easier to carry out the experiments on systems that can show strong magneto-thermopower at relatively low magnetic fields. An experimental study on the magnetic-field-enhanced TE properties of the Dirac semimetal Cd_3As_2 single crystal was reported by Wang *et al.*[102] In the experiments, they found a huge zT of 1.1 at 350 K when applying magnetic fields of up to 7 T.[102] Such a high zT is comparable to that of the best room-temperature TE $Bi_2(Te,Se)_3$ system.[103]

Near room temperature, Cd_3As_2 crystallizes in a tetragonal lattice (space group 142) with a complex unit cell of 160 atoms,[104] as shown in Fig. 5(a). Despite having a complex crystal structure, the electronic structure near the Fermi surface shows a very simple Dirac cone-like shape [Fig. 5(b)], making the charge carrier highly movable in the lattice. An ultrahigh carrier mobility of 9 × 10^6 cm^2 V^{-1} s^{-1} at 5 K was reported in a high-quality single crystal.[70] Even at room temperature, the carrier mobility can still be larger than 10^4 cm^2 V^{-1} s^{-1},[105] indicating that strong response in magneto-transport properties can be realized in Cd_3As_2 even at room temperature. Aside from the high mobility, the complex unit cell generates a group of soft optical phonon branches at the Brillouin zone center in Cd_3As_2,[106] leading to intrinsically low phonon thermal conductivity (below 1 W m^{-1} K^{-1} at 300 K, Fig. 5(c)). Near room temperature, the electron thermal conductivity contributes to more than 60% of the total thermal conductivity, providing a large room for the observation of magnetic field-suppressed thermal conductivity. These intrinsic physical properties make Cd_3As_2 an ideal model system for exploring the magneto-thermoelectric properties of TSMs.

The magneto-TE properties of Cd_3As_2 single crystals with various carrier concentrations have been systematically studied by
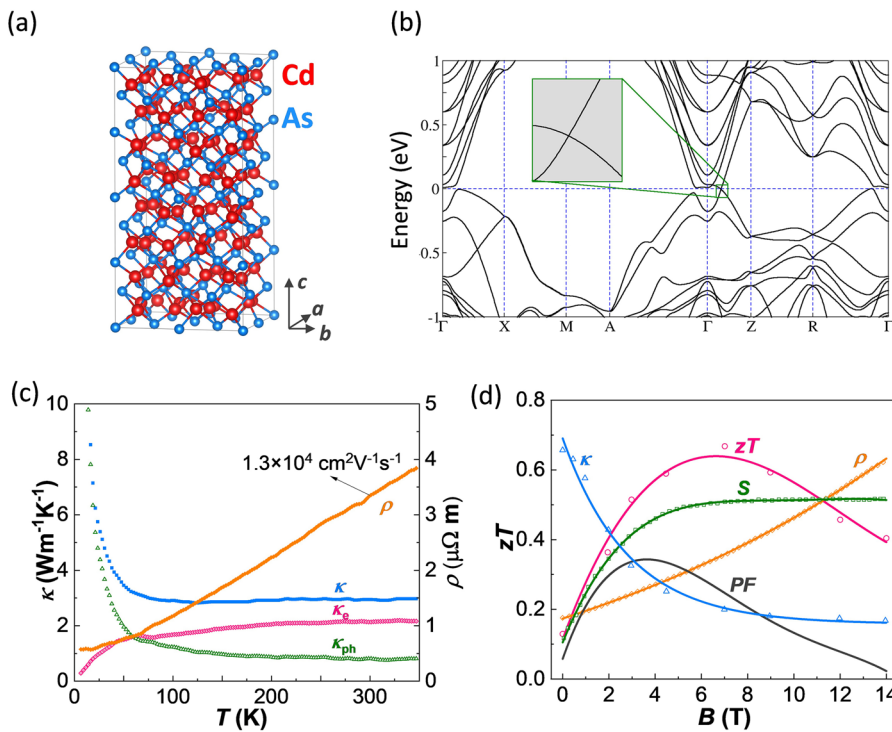
FIG. 5. (a) Crystal structure of Cd_3As_2, drawn using VESTA.[107] (b) Electronic structure of Cd_3As_2. (c) Electrical resistivity and thermal conductivity of the Cd_3As_2 single crystal with a carrier concentration of 1.39×10^{18} cm^{-3}. (d) Room temperature magnetic field-dependent zT in Cd_3As_2; there is a trade-off between the thermal conductivity (κ; plotted on the y-axis from 0 to a top value of 4 W m^{-1} K^{-1}), thermopower (S; -50 $\mu V/K$ to -150 $\mu V/K$), electrical resistivity (0–15 $\mu\Omega$ m), and power factor (10–40 μW cm^{-1} K^{-2}). The discrete data were taken from Ref. 102, while the curves are added for visualizing the trend.

Wang *et al.*[102,105] Here, taking one crystal as an example, the field-dependent transport properties are exhibited in Fig. 5(d). As the magnetic field increases, ρ increases approximately linearly, while the absolute S first increases and then saturates; κ first exhibits a steep drop and then saturates at high magnetic fields. All these changes in the transport properties result in zT peaks at a certain B. Interestingly, these B-dependent TE properties are reminiscent of the n-dependent TE properties in semiconductors (Fig. 2): the effect of increasing B on the TE properties of Cd_3As_2 is similar to that of decreasing n in TE semiconductors. Recalling the optimal n_{opt}, at which the optimal zT is reached for TE semiconductors, there might be a similar quantity, i.e., an "optimal magnetic field," where the maximum $zT(B)$ appears in TSMs. Generally speaking, this increase in the zT of Cd_3As_2 under the magnetic field results from the different effects of the magnetic field on the electrical and thermal transport properties. Because of the existence of dominating small-angle scattering, the magnetoresistance of Cd_3As_2 displays an almost linear increase with B,[105] deviating significantly from the B^2 relationship observed in the other semimetals.[108] However, the κ of Cd_3As_2 exhibits much quicker decay under the magnetic field. These results lead to the strong violation of the WF law in Cd_3As_2: a surprisingly rapid suppression of L under the magnetic field, which consequently leads to the enhancement of zT.[105] Further understanding these experimental results from a theoretical point of view will be helpful for selecting and developing more TSMs for magnetic-field-enhanced TE performances.

Besides the magneto-Seebeck effect, TSMs could also display a strong transverse Nernst effect under a longitudinal temperature gradient and an orthogonal magnetic field. Compared to the TE devices based on the Seebeck effect, which is generally exploited by both n-type and p-type materials to fabricate thermopiles, devices based on the Nernst effect only require one type of material and, thus, are advantageous for practical applications. NbP is one of the first discovered type-I Weyl semimetals.[100,109] It has a simple tetragonal crystal structure with space group $I4_1md$ (No. 109) and is isostructural to the other type-I Weyl semimetals TaAs, TaP, and NbAs, as displayed in Fig. 6(a). The electronic structure of NbP near E_F comprises small quadratic electron and hole pockets and additional electron pockets from linear Weyl bands [Fig. 6(b)].[71] The quadratic electron and hole pockets are similar to those of elemental semimetal Bi. The linear Weyl dispersion usually induces high carrier mobility, as experimentally observed in TSMs.[89] This combination of small quadratic pockets and linear Weyl bands makes NbP a candidate material with a large Nernst effect.

Watzman *et al.* first reported the Nernst effect in the NbP single crystal, which showed a very large Nernst thermopower of about 800 μV K^{-1} at 109 K and 9 T, surpassing the Seebeck thermopower by two orders of magnitude.[110] By combining experimental results and theoretical calculations, they argued that with increasing temperature, the Fermi level shifts toward the energy that has the minimum density of states, contributing to the maximum Nernst thermopower. However, owing to the small size of NbP single crystals (about 2 mm in length direction), it is difficult to measure the magneto-thermal conductivity and evaluate its thermomagnetic performance. Fu *et al.* first synthesized high-quality bulk polycrystalline NbP samples via spark plasma sintering and carried out a systematic study on their magneto-thermoelectric properties and Nernst effect.[111] Although the Nernst thermopower was not as
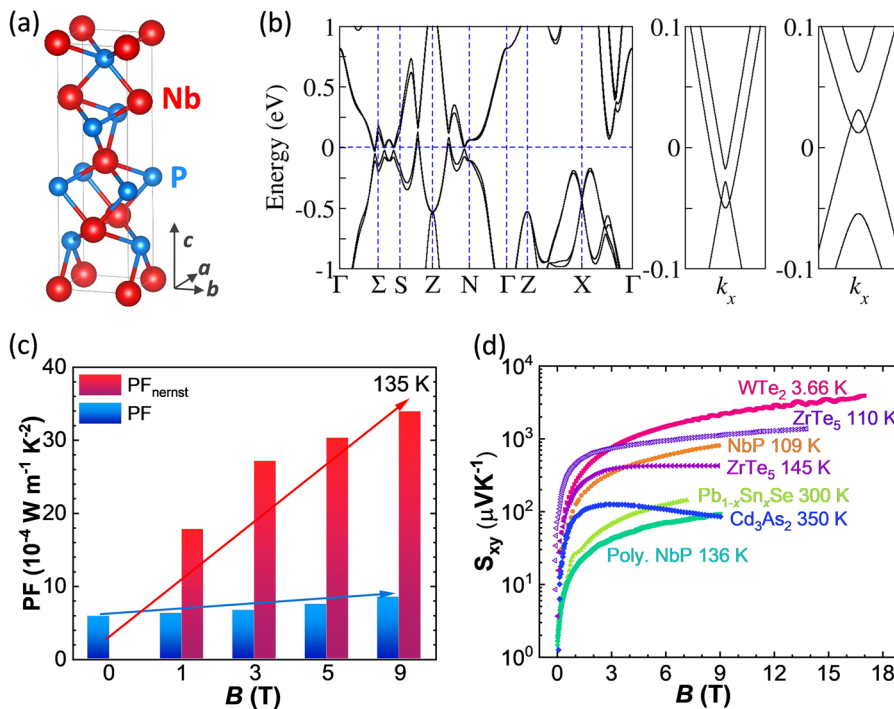
FIG. 6. (a) Crystal structure of NbP, drawn using VESTA.[107] (b) Calculated electronic structure of NbP with quadratic pockets. The two pairs of Weyl points are highlighted separately in the right side since they do not appear at the high-symmetry points of the Brillouin zone. (c) Conventional power factor $S_{xx}^2\sigma_{xx}$ and Nernst power factor $S_{xy}^2\sigma_{yy}$ for polycrystal NbP at 135 K.[111] (d) Nernst thermopower of several TSMs, including single crystalline Cd_3As_2,[91] $Pb_{1-x}Sn_xSe$,[101] NbP,[110] WTe_2,[112] and $ZrTe_5$[113,114] and polycrystalline NbP.[111]

high as that observed in single crystals, the polycrystalline NbP sample still displays a moderate value of about 90 μV/K at 136 K and 9 T. More importantly, the Nernst power factor shows a maximum value of about 35×10^{-4} W m^{-1} K^{-2}, which is four times higher than its conventional power factor [Fig. 6(c)] and is comparable to that of state-of-the-art TE materials. However, the large thermal conductivity of NbP prevents its application as a high-performance thermomagnetic material; further studies on suppressing the lattice thermal conductivity could help to improve the thermomagnetic performance. Despite this, polycrystalline NbP, which is easy to synthesize and whose TE properties show a strong response to magnetic fields, could be taken as a reference system for the transverse Nernst effect studies. Moreover, seeking new TSMs with intrinsically low thermal conductivity could be the direction to achieve better thermomagnetic performances. Some potential candidates, i.e., type-II Weyl semimetal (with titled linear dispersion) WTe_2,[112] and Dirac semimetals Cd_3As_2,[91] $Pb_{1-x}Sn_xSe$,[101] and $ZrTe_5$,[113,114] are shown in Fig. 6(d), of which large Nernst thermopower has been experimentally found. Very recently, Xiang *et al.* have reported a large Nernst zT_N of about 0.5 at room temperature in Cd_3As_2 owing to its intrinsically low thermal conductivity and moderate Nernst effect and resistivity. Importantly, this value was obtained in a relatively small magnetic field of 2 T,[91] which can be produced by current permanent magnets. These current studies on either the magneto-Seebeck effect or the Nernst effect highlight a promising direction to explore non-magnetic TSMs for TE applications.

Magnetic TSMs: Anomalous Nernst effect

The above discussed strong Nernst effect is mainly observed in non-magnetic TSMs under an external applied magnetic field.

In a ferromagnet, the spontaneous magnetization could work as an effective internal magnetic field. Therefore, under a thermal gradient, a ferromagnet could also display a strong transverse voltage response, i.e. ANE.[115,116] There are mainly two contributions to the ANE: the extrinsic contribution from impurity scattering and the intrinsic contribution from the Berry curvature of the electronic structure. Here, we focus on the intrinsic contribution, which has a close relationship with the exotic electronic structure of magnetic TMs.

Similar to Eq. (1), the anomalous Nernst conductivity α_{xy}^A and anomalous Hall conductivity σ_{xy}^A also follow the Mott relation:[117]

$$\alpha_{xy}^A = -\frac{1}{e}\int d\varepsilon \frac{\partial f}{\partial \mu}\sigma_{xy}(\varepsilon)\frac{\varepsilon-\mu}{T}, \quad (3)$$

$$\sigma_{xy}^A = -\frac{2\pi e^2}{h}\int [dk]\Theta(\varepsilon - \varepsilon_k)\Omega_z(k), \quad (4)$$

where f is the Fermi–Dirac function, μ is the chemical potential, and $\Omega_z(k)$ is the Berry curvature, i.e., the Berry phase per unit area in k space. At low temperatures, the relation (3) reduces to

$$\alpha_{xy}^A = \frac{\pi^2}{3}\frac{k_B^2 T}{e}\sigma'_{xy}(E_F). \quad (5)$$

According to the abovementioned equations, large $\Omega_z(k)$ leads to a large σ_{xy}^A, while a strong energy-dependent σ_{xy}^A near E_F is essential to obtain a large α_{xy}^A. The relationship between $\Omega_z(k)$, σ_{xy}^A, and α_{xy}^A is demonstrated in Fig. 7. It is worth noting that σ_{xy}^A reaches the peak value when E_F crosses the Weyl points. In contrast, the maximum α_{xy}^A occurs when E_F shifts away from the Weyl points.
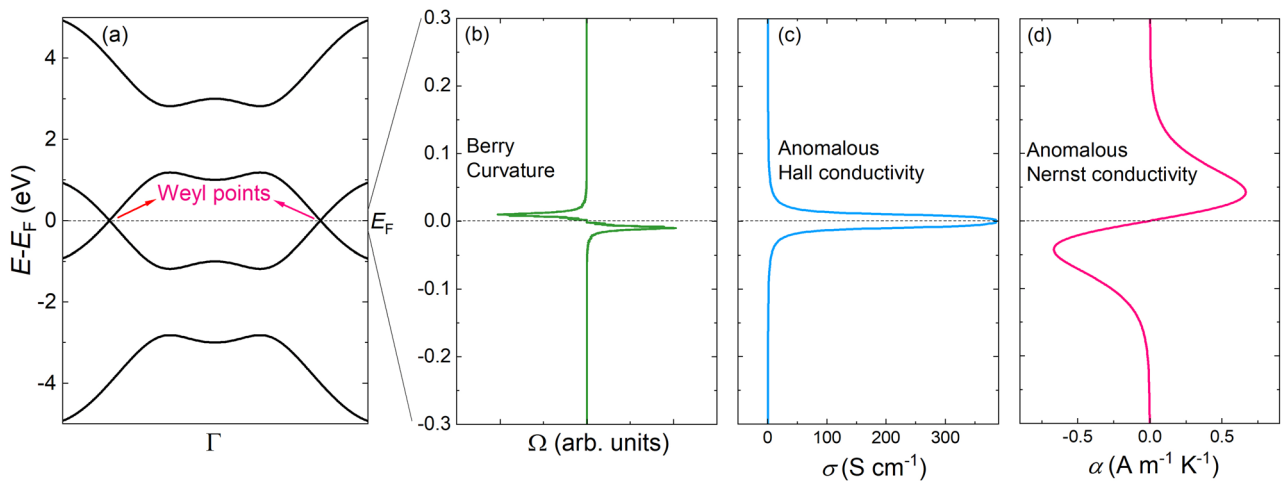
FIG. 7. (a) Band structure with Weyl points on the Fermi level. (b) Berry curvature at fixed energy integrated over the whole Brillouin zone. (c) Anomalous Hall conductivity reaches the peak value when E_F locates at the Weyl points. (d) Anomalous Nernst conductivity reaches the peak value when E_F shifts away from Weyl points.[118]

Therefore, the ANE measurement is also thought of as an effective tool for the characterization of topological band structures in the TMs where E_F deviates from the Weyl points.[118]

Magnetic TMs, especially the recently discovered magnetic Weyl semimetals, namely, the ferromagnetic Heusler compound Co_2MnGa[119–121] and the Shandite $Co_3Sn_2S_2$,[51,52] have exhibited an exotic electronic structure and a large Berry curvature near E_F, which have thus become good candidates to show the Berry curvature-induced ANE. Co_2MnGa crystallizes in a regular Heusler structure with space group $Fm\bar{3}m$. Compared with the inverse Heusler structure ($F\bar{4}3m$), the regular Heusler structure exhibits more mirror plans, as shown in Fig. 8(a). Owing to the mirror symmetry, the band inversion between the bands with an opposite mirror eigenvalue forms more nodal lines, corresponding to a larger Berry curvature.[119] A similar case is also found in the crystal structure of $Co_3Sn_2S_2$ [Fig. 8(b)]. These mirror-plane-protected gapless nodal lines in Co_2MnGa and $Co_3Sn_2S_2$ lead to the discovery of large σ_{xy}^A and the anomalous Hall angle.[50,119] Moreover, the ANE in magnetic Weyl semimetals Co_2MnGa[121–123] and $Co_3Sn_2S_2$[93,124,125] has also been studied recently. Compared to conventional ferromagnets, where the ANE is scaled with magnetization, both Co_2MnGa and $Co_3Sn_2S_2$ show a significantly larger anomalous Nernst thermopower beyond the magnetization scaling relation. Further calculations indicate that these high values of the ANE arise from the large net Berry curvature near E_F associated with nodal lines and Weyl points.[123] Another important example to show the Berry curvature-induced intrinsic ANE is Mn_3Sn, which is an antiferromagnet with almost zero magnetization but shows unexpectedly large ANE[126,127] because of its Berry curvature.[128] Compared to the large, non-saturating Nernst thermopower observed in nonmagnetic TSMs [Fig. 6(d)], the anomalous Nernst thermopower in magnetic Weyl semimetals is still very small. However, the ANE does show significant advantages for potential transverse TE applications as it usually saturates at the relatively low magnetic field (<1 T). Moreover, in some ferromagnetic systems, the ANE effect can occur

even under zero magnetic field, for example, the hard-ferromagnetic Weyl semimetals $Co_3Sn_2S_2$[93] and the diluted magnetic semiconductors $Ga_{1-x}Mn_xAs$,[92] for which, after magnetization, the zero-field anomalous Nernst thermopower was observed below the Curie temperature. These results demonstrated the potential of magnetic TMs
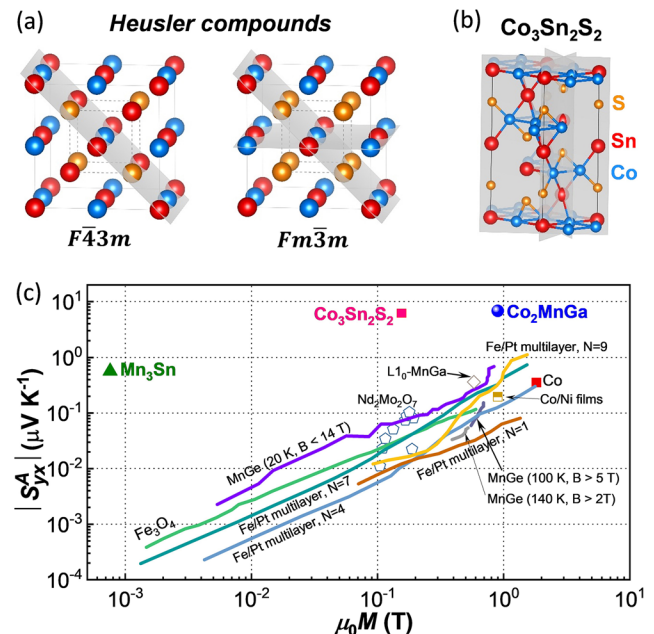

FIG. 8. (a) Heusler compounds with inverse $F\bar{4}3m$ and regular $Fm\bar{3}m$ crystal structures. The mirror planes are shown. (b) Crystal structure of $Co_3Sn_2S_2$ with mirror planes, drawn using VESTA.[107] (c) Magnetization-dependent anomalous Nernst thermopower. Data were adapted from Refs. 93, 123, and 126.

for low-power TE devices based on the ANE. Future development in this direction would rely on the discovery of magnetic TMs with a giant Berry curvature and fine-tuning of the Fermi level.

SUMMARY AND OUTLOOK

The development of TMs has greatly expanded our understanding of solid materials with exotic electronic structures and physical properties, which offers rich opportunities to use these TMs for various TE energy conversion modalities, as demonstrated by recent theoretical and experimental results. Much larger Seebeck and Nernst thermopowers and the violation of the Wiedemann–Franz law have been observed, showing promising ways to improve the upper limit of zT. However, to further promote the development of this emerging topological thermoelectrics field, several scientific and technical challenges need to be overcome.

First, theoretical development to describe and to help understand the topological thermoelectrics, especially the interaction between the TE transport behavior of TMs and either an external magnetic field or spontaneous magnetization, is required. In TSMs, the transport properties are usually contributed by both electrons and holes. Their scattering mechanisms are more complicated than those in the heavily doped TE semiconductors, where only one type of carrier dominates the electrical transport. Second, the Fermi levels for real-world TIs and TSMs are often not located at the Dirac/Weyl points. Therefore, chemical doping and defect-manipulation are important to shift the position of the Fermi level so that the Dirac/Weyl physics can be well understood. The carrier mobility of TSMs strongly relates to the quality of the as-grown single crystals. Therefore, the growth of high-quality crystals is essential to realize the desired functional applications, requiring both scientific and technical insights. Third, the measurements of electrical and thermal transport properties under a magnetic field, especially on anisotropic single crystals of small sizes, are challenging, compared to conventional TE measurements without a magnetic field.

Although the challenges are huge, the exploration of topological thermoelectrics is a very attractive topic. The investigations of the electrical and thermal transport properties with and without a magnetic field could deepen our understanding of the complex transport behavior of quasiparticles in TMs, which could open new ways for developing high-performance TE energy conversion. Moreover, the requirement of high-quality single crystals will boost the development of advanced techniques for crystal growth and characterization. Hence, we are optimistically expecting that more studies on topological thermoelectrics will come targeting both the physical understanding and energy conversion applications of TMs.

REFERENCES

[1] G. J. Snyder and E. S. Toberer, Nat. Mater. **7**, 105 (2008).

[2] J. He and T. M. Tritt, Science **357**, eaak9997 (2017).

[3] H. J. Goldsmid, *Introduction of Thermoelectricity* (Springer, Heidelberg, Germany, 2010).

[4] T. J. Seebeck, Ann. Phys. **82**(3), 253 (1826).

[5] A. F. Ioffe, *Semiconductor Thermoelements and Thermoelectric Cooling* (Infosearch Limited, London, 1957).

[6] L. D. Hicks and M. S. Dresselhaus, Phys. Rev. B **47**, 16631 (1993).

[7] L. D. Hicks and M. S. Dresselhaus, Phys. Rev. B **47**, 12727 (1993).

[8] G. A. Slack, *CRC Handbook of Thermoelectrics* (CRC Press, Boca Raton, 1995).

[9] G. D. Mahan and J. O. Sofo, Proc. Natl. Acad. Sci. U. S. A. **93**, 7436 (1996).

[10] J. P. Heremans, V. Jovovic, E. S. Toberer, A. Saramat, K. Kurosaki, A. Charoenphakdee, S. Yamanaka, and G. J. Snyder, Science **321**, 554 (2008).

[11] Y. Pei, X. Shi, A. LaLonde, H. Wang, L. Chen, and G. J. Snyder, Nature **473**, 66 (2011).

[12] K. Biswas, J. He, I. D. Blum, C.-I. Wu, T. P. Hogan, D. N. Seidman, V. P. Dravid, and M. G. Kanatzidis, Nature **489**, 414 (2012).

[13] L. Hu, T. Zhu, X. Liu, and X. Zhao, Adv. Funct. Maer. **24**, 5211 (2014).

[14] T. Zhu, Y. Liu, C. Fu, J. P. Heremans, J. G. Snyder, and X. Zhao, Adv. Mater. **29**, 1605884 (2017).

[15] G. Tan, L.-D. Zhao, and M. G. Kanatzidis, Chem. Rev. **116**, 12123 (2016).

[16] E. S. Toberer, A. Zevalkink, and G. J. Snyder, J. Mater. Chem. **21**, 15843 (2011).

[17] Y. Pei, H. Wang, and G. J. Snyder, Adv. Mater. **24**, 6125 (2012).

[18] J. Xin, Y. Tang, Y. Liu, X. Zhao, H. Pan, and T. Zhu, npj Quantum Mater. **3**, 9 (2018).

[19] W. Liu, X. Tan, K. Yin, H. Liu, X. Tang, J. Shi, Q. Zhang, and C. Uher, Phys. Rev. Lett. **108**, 166601 (2012).

[20] Y. Pei, A. D. LaLonde, H. Wang, and G. J. Snyder, Energy Environ. Sci. **5**, 7963 (2012).

[21] C. Fu, T. Zhu, Y. Liu, H. Xie, and X. Zhao, Energy Environ. Sci. **8**, 216 (2015).

[22] H. Wang, Y. Pei, A. D. LaLonde, and G. J. Snyder, Proc. Natl. Acad. Sci. U. S. A. **109**, 9705 (2012).

[23] C. L. Kane and E. J. Mele, Phys. Rev. Lett. **95**, 146802 (2005).

[24] B. A. Bernevig, T. L. Hughes, and S.-C. Zhang, Science **314**, 1757 (2006).

[25] M. Z. Hasan and C. L. Kane, Rev. Mod. Phys. **82**, 3045 (2010).

[26] X.-L. Qi and S.-C. Zhang, Rev. Mod. Phys. **83**, 1057 (2011).

[27] B. Yan and C. Felser, Annu. Rev. Condens. Matter Phys. **8**, 337 (2017).

[28] C.-Z. Chang, J. Zhang, X. Feng, J. Shen, Z. Zhang, M. Guo, K. Li, Y. Ou, P. Wei, L.-L. Wang, Z.-Q. Ji, Y. Feng, S. Ji, X. Chen, J. Jia, X. Dai, Z. Fang, S.-C. Zhang, K. He, Y. Wang, L. Lu, X.-C. Ma, and Q.-K. Xue, Science **340**, 167 (2013).

[29] C. R. Rajamathi, U. Gupta, N. Kumar, H. Yang, Y. Sun, V. Süß, C. Shekhar, M. Schmidt, H. Blumtritt, P. Werner, B. Yan, S. Parkin, C. Felser, and C. N. R. Rao, Adv. Mater. **29**, 1606202 (2017).

[30] G. Li, C. Fu, W. Shi, L. Jiao, J. Wu, Q. Yang, R. Saha, M. E. Kamminga, A. K. Srivastava, E. Liu, A. N. Yazdani, N. Kumar, J. Zhang, G. R. Blake, X. Liu, M. Fahlman, S. Wirth, G. Auffermann, J. Gooth, S. Parkin, V. Madhavan, X. Feng, Y. Sun, and C. Felser, Angew. Chem. **131**, 13241 (2019).

[31] G. Li, Q. Xu, W. Shi, C. Fu, L. Jiao, M. E. Kamminga, M. Yu, H. Tüysüz, N. Kumar, V. Süß, R. Saha, A. K. Srivastava, S. Wirth, G. Auffermann, J. Gooth, S. Parkin, Y. Sun, E. Liu, and C. Felser, Sci. Adv. **5**, eaaw9867 (2019).

[32] L. Šmejkal, Y. Mokrousov, B. Yan, and A. H. MacDonald, Nat. Phys. **14**, 242 (2018).

[33] J. P. Heremans, R. J. Cava, and N. Samarth, Nat. Rev. Mater. **2**, 17049 (2017).

[34] D. Hsieh, D. Qian, L. Wray, Y. Xia, Y. S. Hor, R. J. Cava, and M. Z. Hasan, Nature **452**, 970 (2008).

[35] Y. L. Chen, J. G. Analytis, J.-H. Chu, Z. K. Liu, S.-K. Mo, X. L. Qi, H. J. Zhang, D. H. Lu, X. Dai, Z. Fang, S. C. Zhang, I. R. Fisher, Z. Hussain, and Z.-X. Shen, Science **325**, 178 (2009).

[36] L. Fu, Phys. Rev. Lett. **106**, 106802 (2011).

[37] Y. Tanaka, Z. Ren, T. Sato, K. Nakayama, S. Souma, T. Takahashi, K. Segawa, and Y. Ando, Nat. Phys. **8**, 800 (2012).

[38] S.-Y. Xu, C. Liu, N. Alidoust, M. Neupane, D. Qian, I. Belopolski, J. D. Denlinger, Y. J. Wang, H. Lin, L. A. Wray, G. Landolt, B. Slomski, J. H. Dil, A. Marcinkova, E. Morosan, Q. Gibson, R. Sankar, F. C. Chou, R. J. Cava, A. Bansil, and M. Z. Hasan, Nat. Commun. **3**, 1192 (2012).

[39] D. L. Mitchell and R. F. Wallis, Phys. Rev. **151**, 581 (1966).

[40] D. Ben-Ayoun, Y. Sadia, and Y. Gelbstein, J. Alloys Compd. **722**, 33 (2017).

[41] S. Borisenko, Q. Gibson, D. Evtushinsky, V. Zabolotnyy, B. Büchner, and R. J. Cava, Phys. Rev. Lett. **113**, 027603 (2014).

[42] Z. K. Liu, J. Jiang, B. Zhou, Z. J. Wang, Y. Zhang, H. M. Weng, D. Prabhakaran, S.-K. Mo, H. Peng, P. Dudin, T. Kim, M. Hoesch, Z. Fang, X. Dai, Z. X. Shen, D. L. Feng, Z. Hussain, and Y. L. Chen, Nat. Mater. **13**, 677 (2014).

[43] A. J. Rosenberg and T. C. Harman, J. Appl. Phys. **30**, 1621 (1959).

[44] D. P. Spitzer, G. A. Castellion, and G. Haacke, J. Appl. Phys. **37**, 3795 (1966).

[45] D. W. G. Ballentyne and D. R. Lovett, J. Phys. D: Appl. Phys. **1**, 585 (1968).

[46] Q. Li, D. E. Kharzeev, C. Zhang, Y. Huang, I. Pletikosić, A. V. Fedorov, R. D. Zhong, J. A. Schneeloch, G. D. Gu, and T. Valla, Nat. Phys. **12**, 550 (2016).

[47] Y. Zhang, C. Wang, L. Yu, G. Liu, A. Liang, J. Huang, S. Nie, X. Sun, Y. Zhang, B. Shen, J. Liu, H. Weng, L. Zhao, G. Chen, X. Jia, C. Hu, Y. Ding, W. Zhao, Q. Gao, C. Li, S. He, L. Zhao, F. Zhang, S. Zhang, F. Yang, Z. Wang, Q. Peng, X. Dai, Z. Fang, Z. Xu, C. Chen, and X. J. Zhou, Nat. Commun. **8**, 15512 (2017).

[48] T. M. Tritt, N. D. Lowhorn, R. T. Littleton, A. Pope, C. R. Feger, and J. W. Kolis, Phys. Rev. B **60**, 7816 (1999).

[49] R. T. Littleton, T. M. Tritt, J. W. Kolis, D. R. Ketchum, N. D. Lowhorn, and M. B. Korzenski, Phys. Rev. B **64**, 121104 (2001).

[50] E. Liu, Y. Sun, N. Kumar, L. Muechler, A. Sun, L. Jiao, S.-Y. Yang, D. Liu, A. Liang, Q. Xu, J. Kroder, V. Süß, H. Borrmann, C. Shekhar, Z. Wang, C. Xi, W. Wang, W. Schnelle, S. Wirth, Y. Chen, S. T. B. Goennenwein, and C. Felser, Nat. Phys. **14**, 1125 (2018).

[51] N. Morali, R. Batabyal, P. K. Nag, E. Liu, Q. Xu, Y. Sun, B. Yan, C. Felser, N. Avraham, and H. Beidenkopf, Science **365**, 1286 (2019).

[52] D. F. Liu, A. J. Liang, E. K. Liu, Q. N. Xu, Y. W. Li, C. Chen, D. Pei, W. J. Shi, S. K. Mo, P. Dudin, T. Kim, C. Cacho, G. Li, Y. Sun, L. X. Yang, Z. K. Liu, S. S. P. Parkin, C. Felser, and Y. L. Chen, Science **365**, 1282 (2019).

[53] J. Corps, P. Vaqueiro, A. Aziz, R. Grau-Crespo, W. Kockelmann, J.-C. Jumas, and A. V. Powell, Chem. Mater. **27**, 3946 (2015).

[54] L. Müchler, F. Casper, B. Yan, S. Chadov, and C. Felser, Phys. Status Solidi RRL **7**, 91 (2013).

[55] N. Xu, Y. Xu, and J. Zhu, npj Quantum Mater. **2**, 51 (2017).

[56] J. Gooth, G. Schierning, C. Felser, and K. Nielsch, MRS Bull. **43**, 187 (2018).

[57] Y. V. Ivanov, A. T. Burkov, and D. A. Pshenay-Severin, Phys. Status Solidi B **255**, 1800020 (2018).

[58] C. Fu, S. Bai, Y. Liu, Y. Tang, L. Chen, X. Zhao, and T. Zhu, Nat. Commun. **6**, 8144 (2015).

[59] J. Yang, L. Xi, W. Qiu, L. Wu, X. Shi, L. Chen, J. Yang, W. Zhang, C. Uher, and D. J. Singh, npj Comput. Mater. **2**, 15015 (2016).

[60] X. Shi, J. Yang, J. R. Salvador, M. Chi, J. Y. Cho, H. Wang, S. Bai, J. Yang, W. Zhang, and L. Chen, J. Am. Chem. Soc. **133**, 7837 (2011).

[61] L. D. Zhao, H. J. Wu, S. Q. Hao, C. I. Wu, X. Y. Zhou, K. Biswas, J. Q. He, T. P. Hogan, C. Uher, C. Wolverton, V. P. Dravid, and M. G. Kanatzidis, Energy Environ. Sci. **6**, 3346 (2013).

[62] J. Ziman, *Electrons and Phonons* (Oxford University Press, Oxford, 2001).

[63] M. Hong, W. Lyu, Y. Wang, J. Zou, and Z.-G. Chen, J. Am. Chem. Soc. **142**, 2672 (2020).

[64] N. F. Mott and E. A. Davis, *Electronic Processes in Non-Crystalline Materials* (Clarendon, Oxford, 1971).

[65] P. Sun, B. Wei, J. Zhang, J. M. Tomczak, A. M. Strydom, M. Søndergaard, B. B. Iversen, and F. Steglich, Nat. Commun. **6**, 7475 (2015).

[66] D. Shoenberg, *Magnetic Oscillations in Metals* (Cambridge University Press, Cambridge, 1984).

[67] L. D. Landau and E. M. Lifshitz, *Quantum Mechanics: Non-Relativistic Theory*, 3rd ed. (Butterworth-Heinemann, 1981).

[68] P. B. Alers and R. T. Webber, Phys. Rev. **91**, 1060 (1953).

[69] M. N. Ali, J. Xiong, S. Flynn, J. Tao, Q. D. Gibson, L. M. Schoop, T. Liang, N. Haldolaarachchige, M. Hirschberger, N. P. Ong, and R. J. Cava, Nature **514**, 205 (2014).

[70] T. Liang, Q. Gibson, M. N. Ali, M. Liu, R. J. Cava, and N. P. Ong, Nat. Mater. **14**, 280 (2014).

[71] C. Shekhar, A. K. Nayak, Y. Sun, M. Schmidt, M. Nicklas, I. Leermakers, U. Zeitler, Y. Skourski, J. Wosnitza, Z. Liu, Y. Chen, W. Schnelle, H. Borrmann, Y. Grin, C. Felser, and B. Yan, Nat. Phys. **11**, 645 (2015).

[72] E. Mun, H. Ko, G. J. Miller, G. D. Samolyuk, S. L. Bud'ko, and P. C. Canfield, Phys. Rev. B **85**, 035135 (2012).

[73] C. Fu, S. N. Guin, T. Scaffidi, Y. Sun, R. Saha, S. J. Watzman, A. K. Srivastava, G. Li, W. Schnelle, S. S. P. Parkin, C. Felser, and J. Gooth, Research **2020**, 464350.

[74] R. Wolfe and G. E. Smith, Appl. Phys. Lett. **1**, 5 (1962).

[75] A. E. Bowley, R. Delves, and H. J. Goldsmid, Proc. Phys. Soc. **72**, 401 (1958).

[76] Z. Jia, C. Li, X. Li, J. Shi, Z. Liao, D. Yu, and X. Wu, Nat. Commun. **7**, 13013 (2016).

[77] B. Skinnier and L. Fu, Sci. Adv. **4**, eaat2621 (2018).

[78] A. Jaoui, B. Fauqué, C. W. Rischau, A. Subedi, C. Fu, J. Gooth, N. Kumar, V. Süß, D. L. Maslov, C. Felser, and K. Behnia, npj Quantum Mater. **3**, 64 (2018).

[79] D. A. Bandurin, I. Torre, R. K. Kumar, M. Ben Shalom, A. Tomadin, A. Principi, G. H. Auton, E. Khestanova, K. S. Novoselov, I. V. Grigorieva, L. A. Ponomarenko, A. K. Geim, and M. Polini, Science **351**, 1055 (2016).

[80] J. Crossno, J. K. Shi, K. Wang, X. Liu, A. Harzheim, A. Lucas, S. Sachdev, P. Kim, T. Taniguchi, K. Watanabe, T. A. Ohki, and K. C. Fong, Science **351**, 1058 (2016).

[81] P. J. W. Moll, P. Kushwaha, N. Nandi, B. Schmidt, and A. P. Mackenzie, Science **351**, 1061 (2016).

[82] J. Gooth, F. Menges, N. Kumar, V. Süβ, C. Shekhar, Y. Sun, U. Drechsler, R. Zierold, C. Felser, and B. Gotsmann, Nat. Commun. **9**, 4093 (2018).

[83] A. v. Ettingshausen and W. Nernst, Ann. Phys. Chem. **265**, 343 (1886).

[84] K. Behnia and H. Aubin, Rep. Prog. Phys. **79**, 046502 (2016).

[85] H. J. Goldsmid, Br. J. Appl. Phys. **14**, 271 (1963).

[86] T. Aono, Jpn. J. Appl. Phys., Part 1 **9**, 761 (1970).

[87] K. F. Cuff, R. B. Horst, J. L. Weaver, S. R. Hawkins, C. F. Kooi, and G. M. Enslow, Appl. Phys. Lett. **2**, 145 (1963).

[88] M. E. Ertl, D. M. Jacobson, and H. L. Johnson, J. Phys. D: Appl. Phys. **3**, 617 (1970).

[89] J. Hu, S.-Y. Xu, N. Ni, and Z. Mao, Annu. Rev. Mater. Res. **49**, 207 (2019).

[90] X. H. Chen, Sci. China: Phys., Mech. Astron. **63**, 237031 (2019).

[91] J. Xiang, S. Hu, M. Lyu, W. Zhu, C. Ma, Z. Chen, F. Steglich, G. Chen, and P. Sun, Sci. China: Phys., Mech. Astron. **63**, 237011 (2019).

[92] Y. Pu, D. Chiba, F. Matsukura, H. Ohno, and J. Shi, Phys. Rev. Lett. **101**, 117208 (2008).

[93] S. N. Guin, P. Vir, Y. Zhang, N. Kumar, S. J. Watzman, C. Fu, E. Liu, K. Manna, W. Schnelle, J. Gooth, C. Shekhar, Y. Sun, and C. Felser, Adv. Mater. **31**, 1806622 (2019).

[94] D. Xiao, M.-C. Chang, and Q. Niu, Rev. Mod. Phys. **82**, 1959 (2010).

[95] H. Shi, D. Parker, M.-H. Du, and D. J. Singh, Phys. Rev. Appl. **3**, 014004 (2015).

[96] J. Zhang, X. Feng, Y. Xu, M. Guo, Z. Zhang, Y. Ou, Y. Feng, K. Li, H. Zhang, L. Wang, X. Chen, Z. Gan, S.-C. Zhang, K. He, X. Ma, Q.-K. Xue, and Y. Wang, Phys. Rev. B **91**, 075431 (2015).

[97] Y. Xu, Z. Gan, and S.-C. Zhang, Phys. Rev. Lett. **112**, 226801 (2014).

[98] T.-H. Wang and H.-T. Jeng, ACS Appl. Energy Mater. **1**, 5646 (2018).

[99] N. P. Armitage, E. J. Mele, and A. Vishwanath, Rev. Mod. Phys. **90**, 015001 (2018).

[100] S.-Y. Xu, I. Belopolski, N. Alidoust, M. Neupane, G. Bian, C. Zhang, R. Sankar, G. Chang, Z. Yuan, C.-C. Lee, S.-M. Huang, H. Zheng, J. Ma, D. S. Sanchez,

B. Wang, A. Bansil, F. Chou, P. P. Shibayev, H. Lin, S. Jia, and M. Z. Hasan, Science **349**, 613 (2015).

[101]T. Liang, Q. Gibson, J. Xiong, M. Hirschberger, S. P. Koduvayur, R. J. Cava, and N. P. Ong, Nat. Commun. **4**, 2696 (2013).

[102]H. Wang, X. Luo, W. Chen, N. Wang, B. Lei, F. Meng, C. Shang, L. Ma, T. Wu, X. Dai, Z. Wang, and X. Chen, Sci. Bull. **63**, 411 (2018).

[103]L. Hu, H. Wu, T. Zhu, C. Fu, J. He, P. Ying, and X. Zhao, Adv. Energy Mater. **5**, 1500411 (2015).

[104]A. Pietraszko and K. Łukaszewicz, Phys. Status Solidi A **18**, 723 (1973).

[105]H. Wang, X. Luo, K. Peng, Z. Sun, M. Shi, D. Ma, N. Wang, T. Wu, J. Ying, Z. Wang, and X. Chen, Adv. Funct. Mater. **29**, 1902437 (2019).

[106]S. Yue, H. T. Chorsi, M. Goyal, T. Schumann, R. Yang, T. Xu, B. Deng, S. Stemmer, J. A. Schuller, and B. Liao, Phys. Rev. Res. **1**, 033101 (2019).

[107]K. Momma and F. Izumi, J. Appl. Cryst. **44**, 1272 (2011).

[108]B. Fauqué, X. Yang, W. Tabis, M. Shen, Z. Zhu, C. Proust, Y. Fuseya, and K. Behnia, Phys. Rev. Mater. **2**, 114201 (2018).

[109]B. Q. Lv, H. M. Weng, B. B. Fu, X. P. Wang, H. Miao, J. Ma, P. Richard, X. C. Huang, L. X. Zhao, G. F. Chen, Z. Fang, X. Dai, T. Qian, and H. Ding, Phys. Rev. X **5**, 031013 (2015).

[110]S. J. Watzman, T. M. McCormick, C. Shekhar, S.-C. Wu, Y. Sun, A. Prakash, C. Felser, N. Trivedi, and J. P. Heremans, Phys. Rev. B **97**, 161404 (2018).

[111]C. Fu, S. N. Guin, S. J. Watzman, G. Li, E. Liu, N. Kumar, V. Süβ, W. Schnelle, G. Auffermann, C. Shekhar, Y. Sun, J. Gooth, and C. Felser, Energy Environ. Sci. **11**, 2813 (2018).

[112]Z. Zhu, X. Lin, J. Liu, B. Fauqué, Q. Tao, C. Yang, Y. Shi, and K. Behnia, Phys. Rev. Lett. **114**, 176601 (2015).

[113]J. L. Zhang, C. M. Wang, C. Y. Guo, X. D. Zhu, Y. Zhang, J. Y. Yang, Y. Q. Wang, Z. Qu, L. Pi, H.-Z. Lu, and M. L. Tian, Phys. Rev. Lett. **123**, 196602 (2019).

[114]W. Zhang, P. Wang, B. Skinner, R. Bi, V. Kozii, C.-W. Cho, R. Zhong, J. Schneeloch, D. Yu, G. Gu, L. Fu, X. Wu, and L. Zhang, Nat. Commun. **11**, 1046 (2020).

[115]R. Suryanarayanan, V. Gasumyants, and N. Ageev, Phys. Rev. B **59**, R9019 (1999).

[116]M. Mizuguchi and S. Nakatsuji, Sci. Technol. Adv. Mater. **20**, 262 (2019).

[117]D. Xiao, Y. Yao, Z. Fang, and Q. Niu, Phys. Rev. Lett. **97**, 026603 (2006).

[118]J. Noky, J. Gooth, C. Felser, and Y. Sun, Phys. Rev. B **98**, 241106 (2018).

[119]K. Manna, L. Muechler, T.-H. Kao, R. Stinshoff, Y. Zhang, J. Gooth, N. Kumar, G. Kreiner, K. Koepernik, R. Car, J. Kübler, G. H. Fecher, C. Shekhar, Y. Sun, and C. Felser, Phys. Rev. X **8**, 041045 (2018).

[120]I. Belopolski, K. Manna, D. S. Sanchez, G. Chang, B. Ernst, J. Yin, S. S. Zhang, T. Cochran, N. Shumiya, H. Zheng, B. Singh, G. Bian, D. Multer, M. Litskevich, X. Zhou, S.-M. Huang, B. Wang, T.-R. Chang, S.-Y. Xu, A. Bansil, C. Felser, H. Lin, and M. Z. Hasan, Science **365**, 1278 (2019).

[121]A. Sakai, Y. P. Mizuta, A. A. Nugroho, R. Sihombing, T. Koretsune, M.-T. Suzuki, N. Takemori, R. Ishii, D. Nishi-Hamane, R. Arita, P. Goswami, and S. Nakatsuji, Nat. Phys. **14**, 1119 (2018).

[122]H. Reichlova, R. Schlitz, S. Beckert, P. Swekis, A. Markou, Y.-C. Chen, D. Kriegner, S. Fabretti, G. Hyeon Park, A. Niemann, S. Sudheendra, A. Thomas, K. Nielsch, C. Felser, and S. T. B. Goennenwein, Appl. Phys. Lett. **113**, 212405 (2018).

[123]S. N. Guin, K. Manna, J. Noky, S. J. Watzman, C. Fu, N. Kumar, W. Schnelle, C. Shekhar, Y. Sun, J. Gooth, and C. Felser, NPG Asia Mater. **11**, 16 (2019).

[124]W. You, H. Yang, J. Wang, J. Huang, C. Xi, C. Cao, M. Tian, Z.-A. Xu, J. Dai, and Y. Li, Phys. Rev. Mater. **4**, 024202 (2020).

[125]L. Ding, J. Koo, L. Xu, X. Li, X. Lu, L. Zhao, Q. Wang, Q. Yin, H. Lei, B. Yan, Z. Zhu, and K. Behnia, Phys. Rev. X **9**, 041061 (2020).

[126]M. Ikhlas, T. Tomita, T. Koretsune, M.-T. Suzuki, D. Nishi-Hamane, R. Arita, Y. Otani, and S. Nakatsuji, Nat. Phys. **13**, 1085 (2017).

[127]X. Li, L. Xu, L. Ding, J. Wang, M. Shen, X. Lu, Z. Zhu, and K. Behnia, Phys. Rev. Lett. **119**, 056601 (2017).

[128]J. Kübler and C. Felser, Europhys. Lett. **108**, 67001 (2014).